

GRADIENT LIMITING DEFECTS IN 9-CELL CAVITIES EP PROCESSED AND RF TESTED AT JEFFERSON LAB*

R.L. Geng[#], G. Ciovati, A.C. Crawford^{##}, Jefferson Lab, Newport News, VA 23606, U.S.A.

Abstract

Several 9-cell cavities processed by electropolishing (EP) and RF tested at Jefferson Lab are found to be quench-limited. Pass-band mode excitation measurements provide the first clue of candidate cells responsible for the limit. A second RF test with thermometers attached to the equator region of candidate cells (typically only 2 candidates) reveals a hot spot caused by excessive heating of the operational defect and hence determines its location. High resolution optical tools inspect the RF surface corresponding to the hot spot to image and document the defect. All defects in cavities quench limited < 21 MV/m are sub-mm sized irregularities near but outside of the equator EBW. In contrast, no observable irregularities are found in some other cavities that are quench-limited ~ 30 MV/m. These two types of quench limited cavities have different response to a second EP processing. In this paper, we will give a summary of the test results and attempt to catalog the observed defects. An equation for quench gradient is given.

INTRODUCTION

A major focus of today's ILC cavity gradient R&D program is to improve the gradient yield. With the successful application of post-EP cleaning and advanced EP procedures as well as improved cavity assembly practices, field emission due to contaminants from processing chemistry and particulates from cavity handling is much reduced. As a result, for the gradient level up to 35 MV/m, 9-cell cavity limitation due to field emission is significantly reduced. Now, it is possible to observe and understand the impact of gradient limitation due to quench in 9-cell cavities.

Increasing number of new 9-cell cavities processed and RF tested in the past several years allows plotting some preliminary gradient yield curves. Examples based on 9-cell cavities processed and tested at JLab can be found in [1][2]. An outstanding feature of the yield curve is a significant ($> 15\%$) yield drop at ~ 20 MV/m, due to quench limitation. Similar observation can be made from curves based on independent data set from DESY.

Quench is not a new phenomenon at all. Many cases studied previously were found to be triggered by resistive heating of local normal-conducting defects (hence the breakdown threshold is proportional to H^2). The

documented defects responsible for H^2 -driven thermal breakdown at gradient levels of 5-10 MV/m include chemical stains and foreign particles etc. Local repair methods and tools were already developed for successful defect removal and gradient improvement. Raising the RRR value of the bulk niobium has the benefit of delaying the breakdown threshold by thermally stabilizing the operational defects [3].

There are also documented examples of quench-causing defects in which no foreign material is found [4]. Examples include pits, pin-holes or weld spatters. In these cases, there exists a model that quench is triggered by a phase transition from superconducting state to the normal conducting state as a result of the local surface magnetic field exceeding the critical field (hence the breakdown threshold is proportional to H). The exact nature of the critical field in case of RF ($H_{crit,RF}$) is not yet fully clarified. Nonetheless experimental results established a highest peak surface magnetic field of > 200 mT in a 1300 MHz single-cell niobium cavity [5].

There are two possible scenarios as illustrated in Fig. 1 to bring about the H -driven breakdown:

1. Local magnetic field enhancement model. In this model the local surface magnetic field is enhanced due to grain boundary edges, protrusions or pits [6].
2. Local critical field depression model. In this model, the critical field *within the penetration depth* is locally depressed due to impurities, lattice imperfections etc.

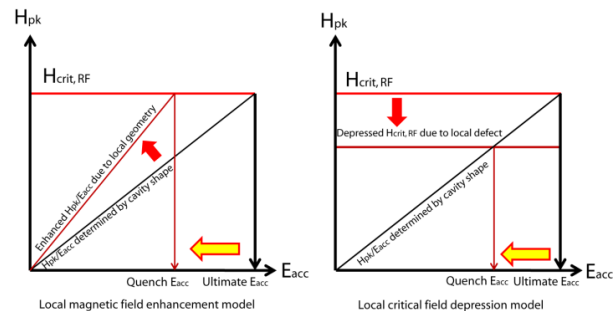


Figure 1: The local magnetic field enhancement model and the local critical field depression model for H -driven thermal breakdown.

METHODS OF QUENCH STUDIES

A 9-cell cavity first goes through the regular qualification processing and testing steps. For those cavities that are clearly quench limited, pass-band mode excitation measurements are performed. This provides the first clue of candidate cells responsible for the quench limit. A second RF test with thermometers [7][8] attached

* Work supported by DOE. Authored by Jefferson Science Associates, LLC under U.S. DOE Contract No. DE-AC05-06OR23177. The U.S. Government retains a non-exclusive, paid-up, irrevocable, world-wide license to publish or reproduce this manuscript for U.S. Government purposes.

[#]geng@jlab.org

^{##}now with FRIB at MSU

to the equator region of candidate pair of cells (as it turned out typically only 2 essential candidate cells) reveals hot spots caused by excessive heating of the operational defect and hence determines their locations. Precursor heating provides additional information about the nature of the defect. High resolution optical tools [9] inspect the RF surface corresponding to the hot spot to image and document the defect. Some cavities are re-processed and tested again for further understanding of the nature of responsible defects.

QUENCH AT GRADIENTS < 20 MV/m

AES1 & AES3 – Insensitivity to Repeated EP

AES1 is the first 9-cell cavity EP processed and RF tested at JLab with a quench limit of 16-18 MV/m [10]. Four RF tests were performed, each after a light EP processing of 16-26 μm . Nevertheless, *the quench limit remained unchanged by repeated processing*. Pass-band measurements were carried out during the 1st, 2nd and 4th RF test. It was shown that the cells #3 & #7 (cell number counted from the input coupler port side) were consistently candidate limiting cells. Later on, cell #3 was singled out to be responsible during RF tests with thermometry at FNAL. Two hot spots were detected at a distance of 7-10 mm from the seam of the equator EBW [7]. Ultimately, AES1 cell #3 RF surface was inspected at KEK using the inspection tool developed by Kyoto University/KEK collaboration [11]. At the location corresponding to hot spots, three circular defects (bumps) (Fig. 2 shows two of them) were observed with a diameter in the range of 400-800 μm and an estimated height of 40-100 μm . It should be noted that AES1 gradient was improved from 16 to 22 MV/m by a 20 μm EP processing at KEK. Nevertheless, the defects in cell #3 remained responsible for the gradient limit and there seemed little changes to their sizes/shapes [12]. This along with previous observation of insensitivity to repeated EP indicates the permanent nature of the responsible defects.

AES3 was quench-limited at 18-21 MV/m despite repeated EP (three times at 23 μm step). Pass-band measurements pointed to cells #4 & #6. RF tests with thermometry determined the quench location to be near but outside the equator EBW of cell #4. AES3 was ultimately inspected at KEK. Within 10 mm distance from the quench location determined by thermometry, a circular defect (probably a bump) with an estimated diameter of 600 μm was observed (Fig. 2).

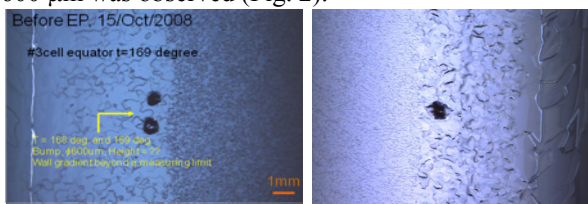


Figure 2: Defects observed near quench site of AES1(L) & AES3(R), limited at 16 & 21 MV/m, respectively. These circular defects have a diameter of ~ 600 μm and are outside the equator EBW (5-10 mm from weld seam).

A15- Limited by Only one Sub-mm Size Defect

A15 was quench-limited at 17-19 MV/m. Pass-band measurements indicated that cells #3 & #7 were candidate limiting cells and *all other cells reached already a peak surface magnetic field of 120-150 mT (equivalent to 28-36 MV/m)*. A second test with two sets of thermometry boards attached to equator regions of cells #3 & #7 determined *the quench location to be only one spot near the equator weld of cell #3* (Fig. 3a). Precursor heating at sensor location (23,7) indicated a drastically increased (still quadratic) heating starting at B_{pk} 55 mT, followed by a departure from quadratic heating at 71 mT (Fig. 3b). It was also noticed that during quench the hottest spot was at sensor location (23,8). Optical inspection with our long-distance-microscope revealed an outstanding circular defect on the RF surface of cell #3 within a distance of 20mm from the quench location predicted by the T-mapping test. The defect has a diameter of 350 μm and is roughly 8 mm from the EBW seam. There is evidence to show that the defect is a pit with an estimated depth of about 170 μm . Fig. 3c gives the image of the defect.

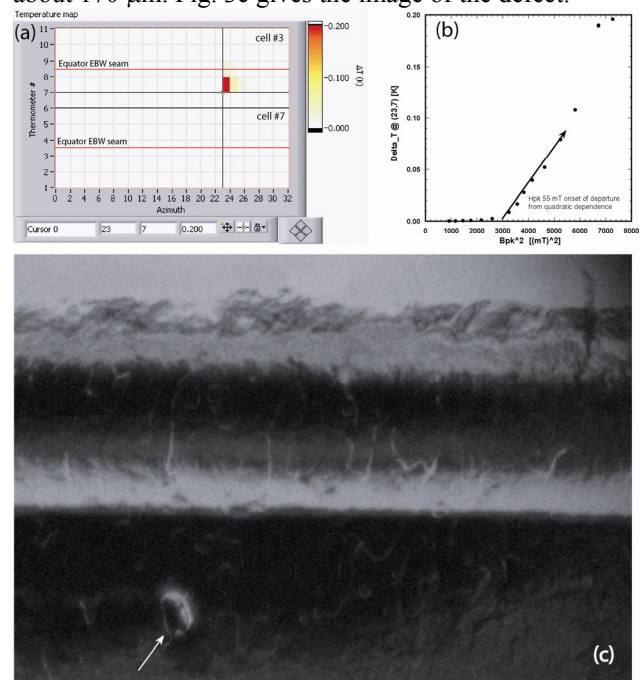


Figure 3: (a) Hot spot in A15 cell #3 just below quench field; (b) Quadratic heating is significantly accelerated at 55 mT followed by a departure from quadratic heating at 71 mT at sensor location (23,7); (c) Defect (indicated by arrow) observed on RF surface within 20 mm distance from the quench site predicted by T-mapping.

AES5 – Again Limited by Only One Defect Limits

AES5 was quench-limited at 20-21 MV/m. Pass-band measurements indicated cells #3 & #7 were candidate limiting cells and *all other cells reached already a peak surface magnetic field of 136-187 mT (equivalent to 32-44 MV/m)*. T-mapping test with thermal sensors attached to equator regions of cells #3 & #7 determined *the quench location to be only one spot near the equator weld of cell*

#3 (Fig. 4a). Sudden temperature rise occurs at B_{pk} 77 mT followed by non-quadratic heating at sensor location (18,9) (Fig. 3b). For comparison, quadratic heating at sensor location (18,2) in cell #7 is clearly shown also in Fig. 3b. Optical inspection revealed an outstanding circular defect on the RF surface of cell #3 within a distance of 10 mm from the quench location predicted by T-mapping. The defect has a diameter of 700 μm and is roughly 8 mm from the EBW seam. The profile of the defect is unclear. Fig. 3c gives the image of the defect.

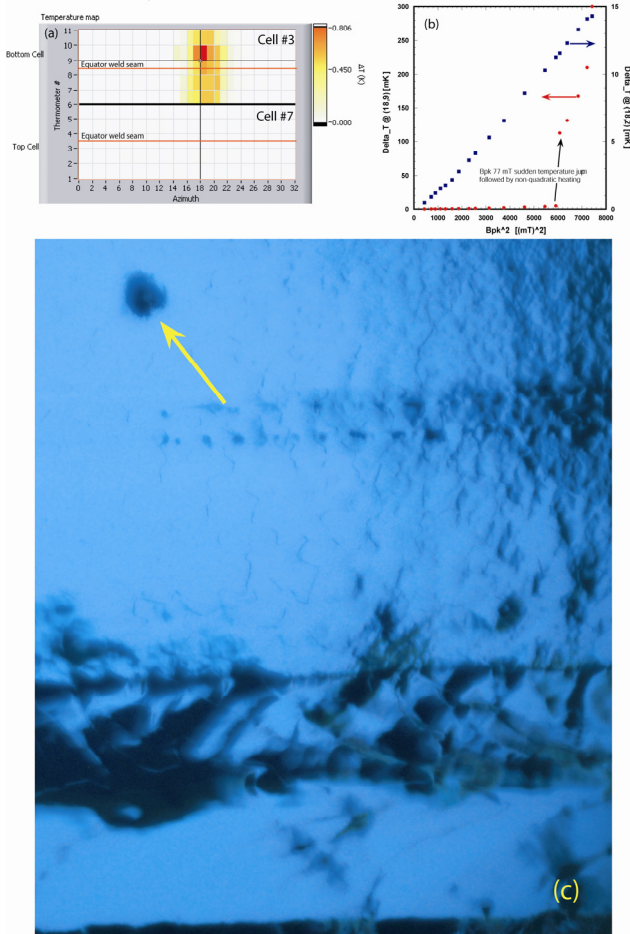


Figure 4: (a) Hot spot in AES5 cell #3 during quench; (b) Sudden temperature rise at B_{pk} 77 mT followed by non-quadratic heating at sensor location (18,9). Quadratic heating at sensor location (18,2) in cell #7 is evident; (c) Defect (indicated by arrow) observed on RF surface within 10 mm from quench site predicted by T-mapping. Full width of the weld is shown in lower portion.

AES6 – Yet Again Limited by Only One Defect

AES6 was quench-limited at 14-15 MV/m. Pass-band measurements indicated cell #5 was the limiting cell and all other cells reached already a peak surface magnetic field of 136-187 mT (equivalent to 32-44 MV/m). T-mapping determined the quench location to be only one spot near the equator weld of cell #5 (Fig. 5a). Initial quadratic heating at sensor location (6,4) was accelerated by a factor of 1.6 at a turning field of 47 mT (Fig. 5b).

Optical inspection revealed outstanding twin defects on the RF surface of cell #5 within a distance of 10mm from the quench location predicted by T-mapping. The defect has a diameter of 300 μm and 500 μm respectively (Fig. 5c) and is roughly 8 mm from the EBW seam. The profile of the defect is unclear.

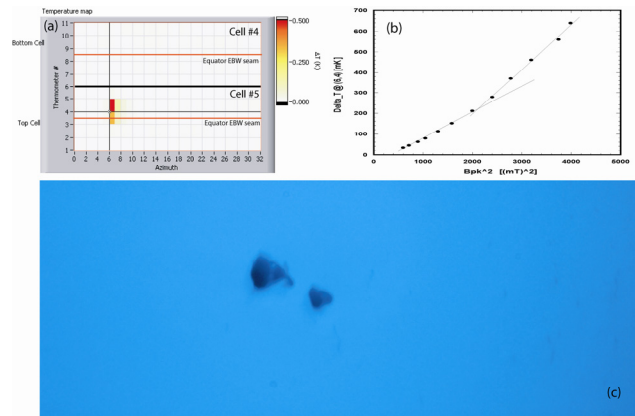


Figure 5: (a) Hot spot in AES6 cell #5 just below quench; (b) Initial quadratic heating at sensor location (6,4) is accelerated at 47 mT B_{pk} ; (c) Twin defects observed on RF surface with 10 mm distance from the quench location predicted by T-mapping.

QUENCH AT GRADIENTS > 30 MV/m

A12

A12 initially reached a maximum gradient of 37 MV/m following the first light EP. During the subsequent handling in preparation for shipping to FNAL, oxide rings were resulted at the high electric field regions of the end cell due to the HPR machine malfunctioning. Oxide rings were successfully removed by immersing the affected area in HF acid. But the cavity performance was only partially recovered and was quench-limited at 32 MV/m (Fig. 6).

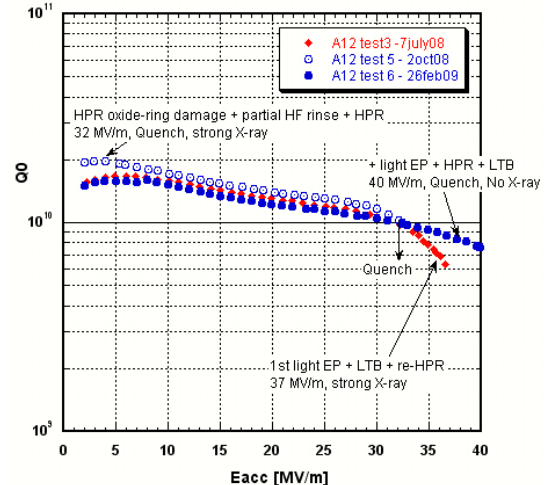


Figure 6: A12 performance and processing history.

Pass-band measurements indicated that cells #3 & #7 are the candidate limiting cells. T-mapping test identified

hot spots below quench field in cell #7 at the sensor location (4,5) and (11,4). The latter, whose location is near the equator EBW, has the highest temperature rise during quench. However, no unusual feature was observed on the RF surface at the location predicted by T-mapping. An extended view of the inspected region is shown in Fig. 7. Finally, A12 was re-processed by 25 μm EP. This recovered and improved the cavity performance to a maximum gradient of 40 MV/m (Fig. 6). This suggests the impermanent nature of the previous limiting defect (probably caused by the HF vapor which is unavoidable during the partial HR immersion for oxide ring removal).



Figure 7: Image of the RF surface at equator region of A12 near quench site. No unusual feature is observable despite the appearance of a quench-correlated hot spot by T-mapping. The quench field was raised from 32 MV/m to 40 MV/m by a light EP processing of 25 μm .

LG1

LG1 is a large-grain 9-cell Nb cavity built by JLab. It was previously tested to a quench limit of 21 MV/m following BCP surface treatment. A light EP of 35 μm was then applied. This raised the quench gradient to 30 MV/m. Pass-band measurements indicated the center cell to be the strongest candidate limiting cell (most remaining cells already reaching a peak surface magnetic field of 140-150 mT). T-mapping of cells #5 & #8 identified the cell #5 quench site to be at the sensor location of (31,8). A departure from quadratic heating at 110 mT is apparent at the quench location (Fig. 8). For comparison, outside the quench site, at the sensor location of (31,2) in cell #8, a clear quadratic heating is evident throughout the field range, despite a much higher absolute temperature rise.

It turns out the quench site coincides with a weld repair performed during fabrication (the last equator EBW). Fig. 9 gives the image of the RF surface at the quench location predicted by T-mapping. It should be noted that similar weld repair was necessary for the equator weld of cell #1. This cell, nonetheless, reached a peak surface magnetic field of 150 mT, inferred from pass-band measurements. There is a possibility that the weld repair in cell #1 was mechanically polished; whereas weld repair in cell #5 was left untouched due to lack of access [13]. A reasonable magnetic field enhancement factor of 1.8 is required to bring about an H-driven thermal breakdown, according to the local magnetic field enhancement model.

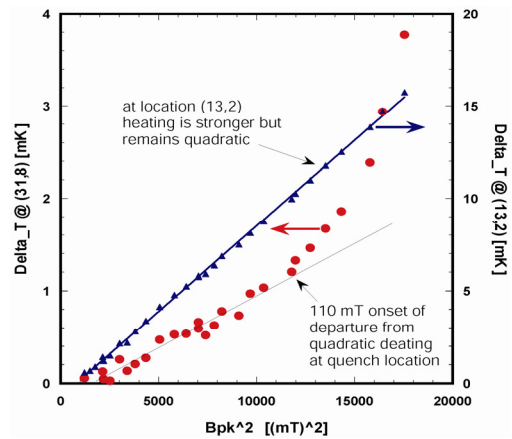


Figure 8: Heating at quench site of LG1 (center cell) departs from quadratic dependence at 110 mT B_{pk} . Outside the quench site, quadratic heating is evident.

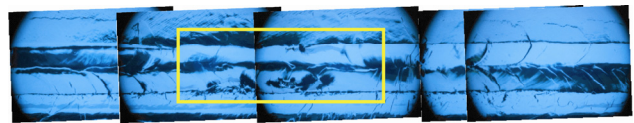


Figure 9: LG1 center cell equator EBW weld repair (boxed region). The quench limit of 30 MV/m is originated from this region, likely brought about by a local magnetic field enhancement effect.

DISCUSSION

As pointed out in [14], the maximum gradient is reduced from the ultimate gradient $H_{crit,RF}/(H_{pk}/E_{acc})$, which is solely determined by the intrinsic material property and cavity geometry, by two effects, namely the *local* magnetic field enhancement and *local* critical field depression (**H**-driven breakdown). As suggested by the precursor heating data shown previously, breakdown does not occur spontaneously at the onset field of local phase transition from superconducting to normal-conducting state, because of thermal stabilization. Taking into account the local magnetic field enhancement effect, local critical field depression effect and thermal stabilization effect, the quench gradient is expressed in the following equation,

$$E_{acc}^{max} = d \cdot \frac{r \cdot H_{crit,RF}}{\beta_{MAG} (H_{pk} / E_{acc})} \quad (1)$$

Here $H_{crit,RF}$ is the intrinsic RF critical field of superconducting material, r is a dimensionless factor representing the reduction of the *local critical field within the penetration depth*, due to impurity or lattice imperfection ($r \leq 1$). β_{MAG} is a dimensionless factor representing the magnetic field enhancement effect due to local geometry ($\beta_{MAG} \geq 1$). H_{pk}/E_{acc} is the peak surface magnetic field to accelerating gradient ratio, determined by cavity shape. d is a dimensionless factor representing the thermal stabilization effect. An improved *local thermal conductivity of bulk material in superconducting state* increases d and the breakdown field is delayed beyond the onset of local phase transition on the RF surface from superconducting to normal conducting.

It is well known that EP smoothes surfaces by preferentially attacking sharp features. As a result, severe protrusions or sharp grain boundaries are unlikely. We estimated a β_{MAG} of 1.8 from the LG1 data. This value is not far away from the calculated value of 1.5 for a semi-sphere [6], so it seems to be reasonable to use it as a reference enhancement factor on electropolished surfaces. Using the A15, AES5 and AES6 data, we estimated a β_{MAG} value of 3.6, 2.6 and 4.3, respectively. Compared to the value of 1.8 from LG1, these values are too high (despite the fact that it is feasible based on calculations in [6]). It seems necessary to invoke also the local critical field depression effect. As a reference, we estimated a depression factor r of 0.7 from the A12 data (in which case, local magnetic field enhancement effect is ruled out for lacking of features at quench site).

SUMMARY

Five cavities (AES1, AES3, A15, AES5 and AES6) EP processed at JLab are quench-limited below 21 MV/m. Major facts are summarized here:

- Outstanding defects, more or less of circular shape with a diameter of 0.3-1 mm, are observed within 10-20 mm distance from the quench location predicted by thermometry.
- There is evidence to show that a defect is a pit (A15) or bump (AES1 & AES3) with a depth/height of < 100 μm . Profiles of defects in AES5 & AES6 are not known.
- Defects are near but outside the complete melted region of the equator EBW. They are not correlated to the overlap of the equator weld. They are 5-10mm distance from the equator weld seam, coinciding with the heat affected zone.
- Repeated EP has little/finite effect on the quench limit (AES1, AES3 and AES6).
- *Only one defect in one cell limits* the entire cavity in A15, AES5 and AES6. Other cells already reached a high E_{acc} of 28-44 MV/m.

We also studied cavities quench limited at > 30 MV/m. One cavity (A12) has no apparent defect at quench site and a light EP cures the limit. One cavity (LG1) is correlated to the center-cell equator weld repair.

We analyzed quench field data based on the **H**-driven thermal breakdown mechanism. An equation for limiting gradient is proposed to reflect three major effects: (1) local magnetic field enhancement; (2) local critical field depression; (3) thermal stabilization. It is suggested that the local magnetic field enhancement effect alone is not sufficient to explain some quench limits < 20 MV/m and it is necessary to invoke the local critical field depression effect. An improvement in thermal conductivity of bulk material at 2-9K (hence phonon peak effect matters) near quench site would delay the quench field.

Presently it is still premature to draw definitive conclusions with regard to the origin of the observed defects responsible for quench limit < 20 MV/m. It is unclear whether there is any reason why cell #3 is more

favorably involved. Microscopic and analytical studies are necessary, even at the cost of sacrificing 9-cell cavities (the chance of having a same defect in 1-cell cavity is much reduced owing to the statistical nature of defect generation). Nevertheless, in recognition of the fact that many cavities are only limited by one sub-mm defect in only one cell with the other cells already reaching very high gradients, a local repair method for defect removal, such as the local electron-beam re-melting method explored at JLab [15], would be an efficient way for performance improvement of these expensive cavities.

ACKNOWLEDGEMENTS

We thank Christiana Grenoble, Pete Kushnick and Michael Morrone for their contribution. RLG is grateful to Hitoshi Hayano and Ken Watanabe of KEK for giving us permission to use the images in Fig. 2.

REFERENCES

- [1] R.L. Geng, "Progress on improving SC cavity performance for ILC", PAC2009, TU3RAI03, (2009).
- [2] R.L. Geng, "Overview of high gradient SRF R&D for ILC cavities at Jefferson Lab", these proceedings.
- [3] H. Padamsee, J. Knobloch, T. Hays, RF Superconductivity for Accelerators, chapter 11& 13, JohnWiley & Sons, Inc., (1998).
- [4] J. Knobloch, "Advanced thermometry studies of superconducting RF cavities", Ph.D. Thesis, Cornell University, 1997.
- [5] R.L. Geng et al., "High gradient studies for ILC with single-cell re-entrant shape and elliptical shape cavities made of fine-grain and large-grain niobium", PAC07, WEPMS006, (2007).
- [6] V. Shemelin, H. Padamsee, "Magnetic field enhancement at pits and bumps on the surface of superconducting cavities", SRF report, SRF080903-04, Cornell University, (2008).
- [7] M. Champion et al., "Quench-limited SRF cavities: failure at the heat-affected zone", ASC2008 (2008).
- [8] G. Ciovati et al., "A 2-cell temperature mapping system for ILC cavities", JLAB-TN-08-012 (2008).
- [9] R.L. Geng et al., "High-gradient SRF R&D for ILC at Jefferson Lab", LINAC08 (2008).
- [10] R.L. Geng et al., "Latest results of high-gradient R&D 9-cell cavities at JLAB", SRF2007, WEP28, (2007).
- [11] Y. Iwashita et al., "Development of a high resolution camera and observation of superconducting cavities", EPAC08, WEOBM03, (2008).
- [12] K. Watanabe, "Optical inspection update at KEK", ILC08, (2008).
- [13] P. Kneisel, private communication.
- [14] R.L. Geng, "Review of new shapes for higher gradients", Physica C, 441, (2006)p145-150.
- [15] R.L. Geng, Bill Clemens, "Exploring defect removal by using local electron beam treatment", these proceedings.